Design and experiment of anti-adhesion rototiller based on staggered double-roller scraping

Jian Cheng[1], Junfang Xia[1,2], Kan Zheng[1,2*], Guoyang Liu[1], Youshuai Wei[1], Juan Zou[3]

(1. *College of Engineering, Huazhong Agricultural University, Wuhan 430070, China*;
2. *Key Laboratory of Agricultural Equipment in Mid-lower Reaches of Yangtze River, Ministry of Agriculture and Rural Affairs, Wuhan 430070, China*;
3. *Hubei academy of agricultural sciences institute of food crops, Wuhan 430070, China*)

Abstract: In order to solve the serious problem of soil adhering blade roller in the middle and lower reaches of Yangtze River, the anti-adhesion rototiller based on staggered double-roller scraping (ARSDS) was designed by mechanical scraping methods. The volume equation for scraping the soil adhesion part with staggered rotary blades was constructed. The mechanical conditions for separation of soil adhesion part from blade roller were clarified, and the contact time between rotary blade and soil during rotary tillage was analyzed. By this way, the key parameters affecting soil adhering on and separating from the blade roller were determined, which were rotational speed, cutting pitch and tillage depth. The spatial and temporal trajectory changes for the sidelong section edge of staggered rotary blades were analyzed, so that the rotary blade arrangement was obtained. Combining the discrete element method, selecting the soil adhesion mass on the staggered blade rollers as the response value established prediction model by Box-Behnken design test. For example, taking the tillage depth of 14 cm for wheat cultivation in the middle and lower reaches of Yangtze River, the optimal combination of parameters was determined to be 230 r/min and 10 cm for rotational speed and cutting pitch, respectively. At this time, the soil adhesion mass was 4566.67 g. In the meantime, the process of soil particles adhering staggered blade rollers and rotary blades scraping off the adhering soil were clarified. Field experiments have shown that the operation quality of ARSDS met the requirements of rototiller performance indexes. In the rice stubble field of high water moisture, the soil adhesion mass was 13.455 kg and 38.215 kg for ARSDS and conventional rototiller, respectively, which indicated that ARSDS effectively reducing soil adhesion mass. The research results can provide technical support for the design of rototiller reducing soil adhesion in the agricultural areas of the middle and lower reaches of the Yangtze River.

Keywords: rice stubble field, rotary tillage, reducing soil adhesion, staggered double-roller, discrete element method
DOI: 10.25165/j.ijabe.20241704.8002

Citation: Cheng J, Xia J F, Zheng K, Liu G Y, Wei Y S, Zou J. Design and experiment of anti-adhesion rototiller based on staggered double-roller scraping. Int J Agric & Biol Eng, 2024; 17(4): 165–175.

1 Introduction

Rotary tillage is an important tillage method in the middle and lower reaches of the Yangtze River agricultural region for water and dry crop rotation systems. It has the advantage of reducing the operation process and saving cost by using rotary tillage operation[1]. Rice is grown under long-term submerged irrigation, and its unique irrigation scheme and alternating wet and dry conditions make soil highly dynamic[2,3]. At the same time, paddy fields are affected by natural and human factors such as seasons, tillage, planting, and fertilization, which produce changes in physical and chemical properties[4]. Therefore, in dry farming, the soil of rice stubble field is sticky and heavy, easy to adhere, and highly plastic, resulting in serious problems of soil adhesion to the blade roller of rototiller.

Surface energy, water film tension, and other chemical properties among soil components contribute to soil adhesion formation, leading to the development of an adhesion system interface between soil and the material surface of the tillage component[5,6]. In highly moist clayey soil, soil adhesion can augment tillage resistance by 30% and elevate energy consumption by 30% to 50%[7]. Given the challenges posed by the considerable work resistance resulting from soil adhesion to tillage components, current research primarily aims to disrupt the adhesion equilibrium between soil and materials contact surfaces, facilitating soil detachment. Mechanical detachment technology involves adding scrapers or other scraping components to the original machinery, or utilizing vibration to dislodge soil adhered to tillage components during soil stripping. For instance, Luo et al.[8] installed a scraper aligned with the ground wheel behind the residual film recycling device, effectively removing soil adhering to the wheel during operation. Liu et al.[9] quantified soil-metal adhesion interface system characteristics following vibration and assessed the impact of vibration parameters on detachment efficacy in both normal and tangential adhesion interfaces. Furthermore, employing morphological technology to replicate animal characteristics, leveraging the benefits of biological morphology and drag-reducing movement traits, enables targeted optimization in designing relevant

Received date: 2022-10-23 **Accepted date:** 2024-05-07
Biographies: **Jian Cheng**, PhD candidate, research interest: agricultural equipment design and control, Email: chengjiancj@webmail.hzau.edu.cn; **Junfang Xia**, PhD, Professor, research interest: straw returning technology and equipment, Email: xjf@mail.hzau.edu.cn; **Guoyang Liu**, PhD candidate, research interest: agricultural equipment design and control, Email: lgy@webmail.hzau.edu.cn; **Youshuai Wei**, MS candidate, research interest: agricultural equipment design and control, Email: 1728043050@qq.com; **Juan Zou**, PhD, associate researcher, research interest: physiology of wheat cultivation, Email: zoujuan1010@163.com.

***Corresponding author: Kan Zheng**, PhD, Associate Professor, research interest: agricultural intelligent equipment。 College of Engineering, Huazhong Agricultural University, No.1, Shizishan Street, Hongshan District, Wuhan 430070, China. Tel: +86-15271890761, Email: zhengkan@mail.hzau.edu.cn.

components. For example, the furrow opener, modeled after the corrugated shape of an earthworm's surface[10], and the bionic cutter teeth prototype, inspired by badger claw toes[11], demonstrate effective adhesion reduction. Concurrently, surface engineering techniques involve coating ultra-high molecular weight polyethylene[12] and applying nano-coating[13] to soil-touching component surfaces, altering the adhesion system's contact state to enhance surface self-cleaning capabilities. The aforementioned research is primarily applied to tillage machinery such as suppression roller and deep loosener. However, rototiller, during operation, undergoes high-speed rotation, impacting, cutting, and throwing soil. This intricate motion process has led to relatively limited research on the correlation between adhesion reduction and rototiller.

Presently, research in rotary tillage operation primarily centers on optimizing the design of rotary blade and blade roller. In the realm of rotary blade research, Matin et al.[14] concluded that the straight blade required the least operating power among three different rotary blades. Additionally, researchers imitate the structure and functional mechanisms of living organisms, such as the claw toe of gryllotalpa[15] and the low-resistance bear paw[16]. Experimental design methodology is employed to optimize rotary blade design by integrating the discrete element method with field experiments. In blade roller research, Li et al.[17] developed a vertical shaft type blade roller inspired by vertical milling characteristics, exhibiting advantages such as low power consumption. Hu et al.[18] constructed a simulation model of double-roller rototiller to investigate the effect of configuration parameters on power consumption. These research findings have established a basis for designing high-quality rototiller, with research objectives centered on reducing drag and consumption, while lacking related studies on adhesion reduction. Consequently, the issue of soil adhesion in rototiller during high-moisture paddy soil operations remains to be addressed.

In this study, the ARSDS was proposed for reducing soil adhesion. By conducting theoretical analyses of critical components, we identified key parameters influencing soil adherence and detachment from the blade roller. Utilizing the discrete element method, we examined the impact of key parameters on soil adhesion mass and the process of soil removal from the blade roller. Additionally, field experiments were conducted to validate the machine's performance. This study provides a reference for rototiller to reduce soil adhesion in the agricultural areas of the middle and lower reaches of the Yangtze River.

2 Machine structure and working principle

2.1 Machine structure

As shown in Figure 1, the machine structure was mainly consisted of frame, transmission box, blade rollers, etc. The suspension frame was mounted on tractor through the pin and three-point suspension assembly. The left and right side transmission boxes were fixed to the side frame to ensure the balance of the machine operation. The rotary blades on the front and rear blade roller were arranged in a staggered manner, and the bending direction of two rotary blades on each cross section was opposite.

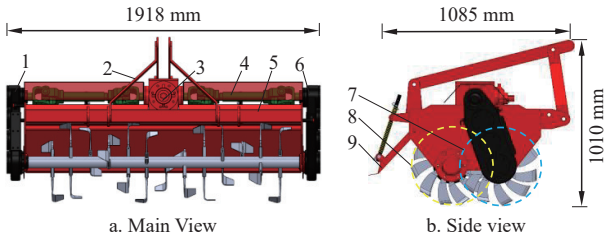

1. Left side transmission 2. Suspension 3. Gearbox 4. Universal joint 5. Frame 6. Right side transmission 7. Front cutter roller 8. Rear cutter roller 9. Fender

Figure 1 Structural diagram of the ARSDS

2.2 working principle

The working principle of the ARSDS is shown in Figure 2. When working in rice stubble field, the tractor output shaft transmitted the power to gearbox to drive the blade rollers rotation. The machine made uniform linear motion to cultivate the soil in the untilled area. Then, the blade rollers cut and squeezed the soil after entering the soil, and thrown the soil backward in the exit and return stage. Rotary blades installed on the single blade roller were spaced on the staggered blade rollers of the ARSDS, which form a staggered arrangement. The distance between the two blade holder on the front and rear knife rollers was enlarged to improve the circulation of the thrown soil. It will prevent soil accumulation to form soil adhesion part, thus affecting the operation effect. Staggered blade rollers were installed at the same level to ensure consistent tillage depth. The rotary motion of the staggered rotary blades formed a closed cylindrical space, which interacted with the soil adhesion part. Mechanical scraping methods was adopted to scrape and disturb the stable cylindrical soil adhesion part. The rotary blades on the front blade roller cut soil adhesion part on the rear cutter roller, and the rotary blades on the rear blade roller soil adhesion part on the front cutter roller. By this way, the adhering soil was removed and ensured that the soil did not adhere and gather on the blade rollers. Eventually, the effect of reducing soil adhesion was achieved.

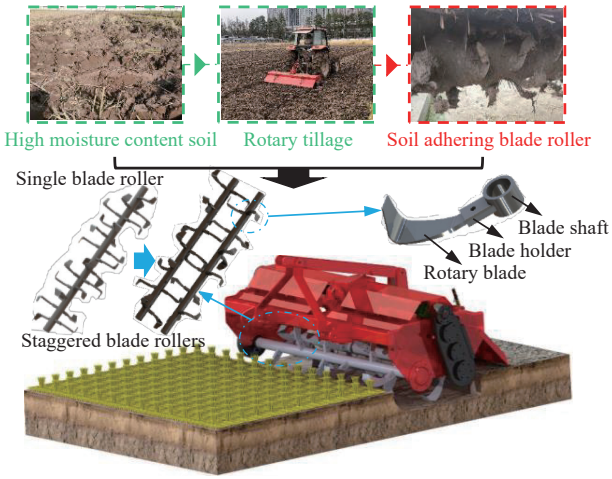

Figure 2 Working principle of the ARSDS

3 Mechanical analysis and parametric design

3.1 Analysis of the soil volume that was scraped by staggered rotary blade

Wet and sticky soil in rice stubble field adheres to the blade roller and is not easy for dropping off. Soil accumulation forms a stable cylindrical soil adhesion part. During tillage, the volume of soil adhesion part scraped by rotary blade affects soil separating from the blade roller. Therefore, it is necessary to construct a parametric equation for the volume of soil adhesion part scraped by the rotary blade, so as to clarify the key parameters affecting the soil adhesion part scraped. As shown in Figure 3a, the coordinate system was established at the center point O_1 of the front blade shaft, with the forward direction of machine as the X_1-axis and the vertical surface direction as the Y_1-axis. The front and rear blade

rollers were fixed to the frame without relative translational motion. When the front and rear blade rollers rotate counterclockwise at the same angular velocity ω, the scraping volume was the volume of soil adhesion part on front blade roller scraped by the rotary blade mounted on the rear blade roller. To facilitate the calculation of scraped volume, the double-roller fixed axis rotation could be equated to the planetary wheel system motion of rear blade roller around the front blade roller. We assume that the soil adhesion part on front blade roller was stationary. The rotary blade on the rear blade roller takes the center point of front blade shaft O_1 as the center, and the center distance between front and rear blade shafts l_1 is the radius revolving clockwise around O_1. At the same time, the center point of rear blade shaft O_2 as the center of the circle, the distance from the rotary center of rotary blade to the sidelong section edge w was the radius of counterclockwise autorotation. In the above description, w is the variable ($q \le w \le R$), q is the distance from the rotary center to the bending line of rotary blade, and R is the rotary radius of rotary blade. According to the translation wheel system theorem, the angular velocity of the revolution was ω and the angular velocity of the autorotation was 2ω.

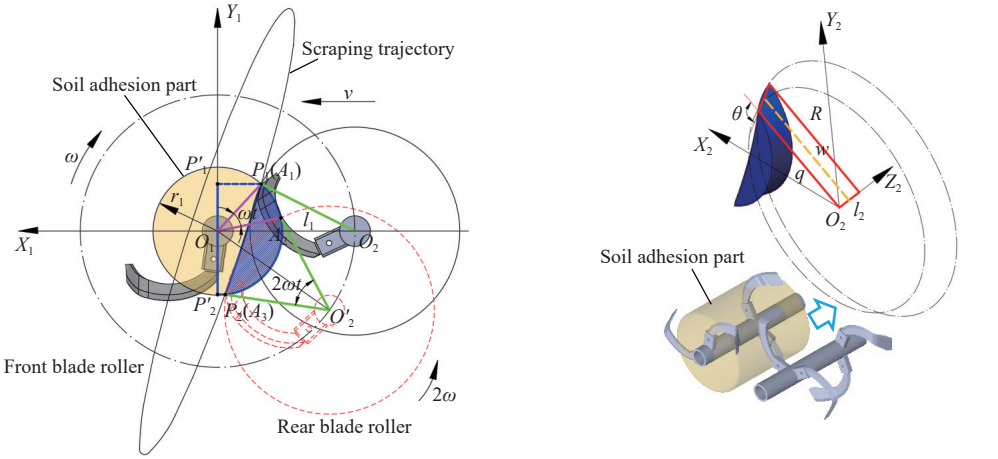

a. Rotary blade scraping area of soil adhesion part b. Rotary blade scraping volume of soil adhesion part

Figure 3 Volume analysis of soil adhesion part scraped by staggered rotary blade

The rotary blade started scraping the soil adhesion part at point A_1 and finished scraping at point A_3. The center point O_2 of rear blade shaft rotated clockwise to O_2' after the time t (t>0), and the rotation angle was ωt. Point A_2 rotated to point A_3 with angular velocity 2ω in counterclockwise direction after t time, and the angle of rotation was $2\omega t$, where point A_2 is the position of point A_1 in the case of autorotation but not revolution. By using the complex number operation and the geometric meaning of complex vector rotation, the following could be obtained:

$$\begin{cases} \overline{O_1O_2'} = l_1[\cos(-\omega t) + i\sin(-\omega t)] \\ \overline{O_2'A_2} = w[\cos(\pi - \omega t) + i\sin(\pi - \omega t)] \\ \overline{O_2'A_3} = \overline{O_2'A_2}(\cos 2\omega t + i\sin 2\omega t) = -w_2(\cos\omega t + i\sin\omega t) \\ \overline{O_1A_3} = \overline{O_1O_2'} + \overline{O_2'A_3} \end{cases} \tag{1}$$

The parameter equation of point A_1 in the coordinate system was obtained by combining Equation (1), as well as the shape of cylindrical soil adhesion part was circular. After transforming the coordinate system, the equation for the trajectory of rotary blade cutting was given as ψ_1 and the equation of soil adhesion part is given as ψ_2.

$$\begin{cases} x_1 = (l_1 - w)\cos(-\omega t) \\ y_1 = (l_1 + w)\sin(-\omega t) \\ x_1 = \psi_1(y_1) = (l_1 - w)\sqrt{1 - \dfrac{y_1^2}{(l_1 + w)^2}} \\ x_2 = \psi_2(y_2) = \sqrt{w^2 - y_2^2} \end{cases} \tag{2}$$

where, r_1 is radius of soil adhesion part, mm.

As shown in Figure 3a, in half a cycle, the area S (blue area) where the rotary blade scraped the soil was the sum of the blue and yellow areas enclosed by points P_1, P_2, P_2' and P_1' (large curved edge trapezoid area S_1) minus the yellow area enclosed by the same points (small curved edge trapezoid area S_2). The area S was obtained as follows:

$$S = S_1 - S_2 = \int_{y_2}^{y_1}\left[\int_0^{x_2(y_2)} \mathrm{d}x - \int_0^{x_1(y_1)} \mathrm{d}x\right]\mathrm{d}y \tag{3}$$

where, y_1 and y_2 are the y-axis coordinates of points P_1 and P_2, mm.

Figure 3b shows the volume of soil adhesion part scraped by single rotary blade. It was assumed that the bending angle θ of rotary blade was obtuse, the rotary blade width is l_2. The distance from the rotary center of rotary blade to the sidelong section edge w gradually increased with the distance to the rotary radius R. In consequence, the geometric relationship between r_2 and the volume of soil adhesion part scraped V was solved as follows:

$$\begin{cases} w = R - \tan(\theta - 90^\circ)l_2 \\ V = \int_0^{l_2} S\,\mathrm{d}l \end{cases} \tag{4}$$

From the above analysis, it was clear that the volume of soil adhesion part scraped V was related to the parameters R, r_2, θ, l_1, and l_2. In actual processing and manufacturing, the rotary radius R was the standard size. Thus, the standard rotary blade with a larger rotary radius was selected, and its rotary radius R was 265 mm. When the rotary blade bending angle θ for 90°, the distance from the rotary center of rotary blade to the sidelong section edge w taken a great value, q=w=R, which could increase the volume of soil adhesion part scraped V. Hence, the bending angle θ was designed to be 90° in this design. The radius of blade shaft was 70 mm, and rotary radius R was 265 mm. When the rotary blade was tangent to the blade shaft, the center distance between the two shafts was 300 mm. Considering the influence of machining error, the center distance between front and rear blade shafts l_1 was determined to be 310 mm. Increasing the rotary blade width l_2 could improve the volume of soil adhesion part scraped V. However, if the rotary blade width l_2 was too long, the operation power consumption will

increase, so the rotary blade width l_2 was determined to be 70 mm. The above analysis effectively maximized the volume where the rotary blade scraped soil adhesion part and improved the soil detachment effect in rice stubble field.

3.2 Mechanical analysis of adhering and separating for soil with blade roller

In rice stubble field, the mechanical conditions of adhering soil to separate from the blade roller are not only associated with the volume of soil adhesion part, but also closely related to the soil material properties and working parameters of blade roller. The adhering soil on blade roller is an elastoplastic material[19], which is divided into elastic and plastic zones during the process of being subjected to rotational motion and scraping. In order to determine the mechanical conditions that destroy the stability of adhering soil, the mechanical analysis of soil was carried out. As shown in Figure 4, the soil adhered to the single blade roller of conventional rototiller rotating. Assuming that the soil adhesion part was made of an ideal elastoplastic material with a yield limit of σ_s. r=c(r_2≤r≤r_1) was denoted as the boundary between the plastic and elastic zones. When the elastic limit angular velocity ω=ω_1, the edge of soil adhesion part at r=r_2 yielded, where r_2 is inner diameter of soil adhesion part. When the plastic limit angular velocity ω=ω_1, the soil adhesion part all yielded. Therefore, the soil adhesion part was elastic-plastic state at the angular velocity of ω_1–ω_2.

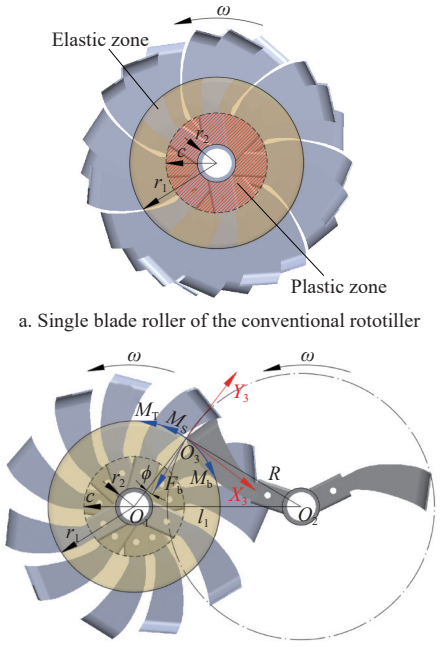

a. Single blade roller of the conventional rototiller

b. Staggered blade rollers

Figure 4 Mechanical analysis of soil adhesion part separating from the blade roller

In the plastic zone r_2<r<c, there should be σ_θ>σ_r>0, where σ_θ is the circumferential stress and σ_r is the radial stress. Based on the Tresca yield condition σ_θ=σ_r, the yield condition was brought into the equilibrium equation[20], and we could obtain the radial stress σ_r. In Equation (5), the first equation represents the expression of the equilibrium equation, while the second equation represents the expression for the radial stress σ_r.

$$\begin{cases} \dfrac{\mathrm{d}}{\mathrm{d}r}(r\sigma_r)=\sigma_s-\rho\omega^2r^2 \\ \sigma_r=\sigma_s-\dfrac{\rho\omega^2r^2}{3}+\dfrac{C}{r} \end{cases} \tag{5}$$

When r=r_2 and σ_r=0, the value of the constant term C was obtained. Meanwhile, the radial stress σ_r could be solved.

$$\begin{cases} C=-r_2\left(\sigma_s-\dfrac{\rho\omega^2r_2^2}{3}\right) \\ \sigma_r=\sigma_s\left(1-\dfrac{r_2}{r}\right)-\dfrac{\rho\omega^2}{3}\left(r^2-\dfrac{r_2^3}{r}\right) \end{cases} \tag{6}$$

In the elastic zone c<r<r_1, the expression of stress could be obtained from the boundary condition and the continuity condition of stress at the elasto-plastic junction. The boundary conditions were: σ_r=0 for r=r_2 or r=r_1. The continuity conditions for the stresses were $(\sigma_r)_e$=$(\sigma_r)_p$ and $(\sigma_\theta)_e$=$(\sigma_\theta)_p$ at r=c, where $(\sigma_r)_e$ is the obtained σ_r in the elastic zone and $(\sigma_r)_p$ is the obtained σ_r in the plastic zone. At this time, the radial stress σ_r and the circumferential stress σ_θ in the elastic zone were

$$\begin{cases} \sigma_r=\sigma_s\left(1-\dfrac{r_2}{2c}-\dfrac{r_2c}{2r^2}\right)+\rho\omega^2\left[\dfrac{c^2}{6}\left(\dfrac{r_2^3}{c^3}+\dfrac{1+3\mu}{2}\right)+\right. \\ \qquad \left.\dfrac{c^4}{6r^2}\left(\dfrac{r_2^3}{c^3}-\dfrac{1+3\mu}{4}\right)-\dfrac{3+\mu}{8}r^2\right] \\ \sigma_\theta=\sigma_s\left(1-\dfrac{r_2}{2c}+\dfrac{r_2c}{2r^2}\right)+\rho\omega^2\left[\dfrac{c^2}{6}\left(\dfrac{r_2^3}{c^3}+\dfrac{1+3\mu}{2}\right)-\right. \\ \qquad \left.\dfrac{c^4}{6r^2}\left(\dfrac{r_2^3}{c^3}-\dfrac{1+3\mu}{4}\right)-\dfrac{1+3\mu}{8}r^2\right] \end{cases} \tag{7}$$

where, μ is Poisson's ratio; ρ is soil density, kg/m³.

According to the above analysis, the limit angular velocity ω_1 and ω_2 could be obtained in the elastic and plastic limit states.

$$\begin{cases} \omega_1=\sqrt{\dfrac{4\sigma_s}{\rho\left[(1-\mu)r_2^2+(3+\mu)r_1^2\right]}} \\ \omega_2=\sqrt{\dfrac{3\sigma_s}{\rho\left[r_1^2+r_2r_1+r_2^2\right]}} \end{cases} \tag{8}$$

With the rotation of staggered blade rollers, it was assumed that the accumulation of adhering soil on the front blade roller forming a cylindrical soil adhesion part. The mechanical conditions of rotary blade scraping the soil were solved according to the limit torque under the elastic-plastic condition. The shear stress distribution on the interface of soil adhesion part in the elastic-plastic state was shown as follows:

$$\begin{cases} \tau=\tau_s\dfrac{r}{c},\ (r_2\le r\le c) \\ \tau=\tau_s,\ (c\le r\le r_1) \end{cases} \tag{9}$$

where, τ_s is shear yield strength, MPa.

The expression of torque M in the elastic-plastic state was obtained by using the static equilibrium condition. When the demarcation line of the elastic-plastic zone was in the inner circle of the annular interface (c=r_2), the torque acting on the soil adhesion part reached the plastic limit torque M_T. Bringing c=r_2 into the expression of torque M, we could get the limit torque M_T.

$$\begin{cases} M=\displaystyle\int_{r_2}^{c}2\pi\tau_s\frac{r^3}{c}\mathrm{d}r+\int_{c}^{r_1}2\pi\tau_sr^2\mathrm{d}r=\frac{2}{3}\pi\tau_sr_1^3\left\{1-\right. \\ \qquad \left.\dfrac{1}{4}\left(\dfrac{c}{r_1}\right)^3\left[1+3\left(\dfrac{r_2}{c}\right)^4\right]\right\} \\ M_T=\dfrac{2}{3}\pi\tau_s\left(r_1^3-r_2^3\right) \end{cases} \tag{10}$$

The torque M_b exerted by the rotary blade on the soil was generated by the force F_b applied by the rotary blade on the soil. In addition, the soil adhesion part was subjected to torque M_s caused

by rotation. The intersection point O_3 of the rotary blade and the soil adhesion part was the coordinate origin. The line between intersection point O_3 and the center point of front blade shaft O_1 was the Y_3-axis, and the tangent line to the soil adhesion part was the X_3-axis. According to the principle of torque superposition, the mechanical conditions for the destruction of the soil adhesion part were determined.

$$\begin{cases} M_b - M_T - M_s > 0 \\ M_b = F_b r_1 \sin\phi = m_1 R r_1 \dfrac{d\omega}{dt} \sin\phi \\ M_s = \dfrac{1}{2} m_2 (r_1^2 + r_2^2) \dfrac{d\omega}{dt} \\ \phi = \arccos\left(\dfrac{r_1^2 + R^2 - l_1^2}{2 r_1 R} \right) - 90^\circ \end{cases} \tag{11}$$

where, m_1 is rotary blade mass, kg; m_2 is soil adhesion part mass, kg; ϕ is the angle between the force F_b and the Y_3-axis, (°).

From the above equation, it could be seen that the limit angular velocities ω_1 and ω_2 were related to σ_s, μ, ρ, r_1 and r_2 when the soil adhering to the single blade roller of conventional rototiller rotating. The soil was adhered to the blade roller, so the inner diameter of soil adhesion part r_2 coincided with the radius of blade shaft. The radius of soil adhesion part r_1 was a random variable that cannot be measured, and soil yield limit σ_s, Poisson's ratio μ and soil density ρ were material properties. Larger soil yield limit σ_s or smaller Poisson's ratio μ and soil density ρ lead to larger limit angular velocities ω_1 and ω_2. An angular velocity ω greater than the limit angular velocity ω_2 in the plastic limit state will destabilize the soil and made it easier for the adhering soil to separate from blade roller. The mechanical conditions for the destruction of the soil adhesion part are related to τ_s, m_1, m_2, ϕ, and ω, of which the shear yield strength τ_s and rotary blade mass m_1 are material properties. The soil adhesion part mass m_2 changed continuously during tillage, while the uncertainty in the radius of soil adhesion part r_1 led to angle ϕ also being a variable. The torque M_b of rotary blade acting on the soil adhesion part at a given moment was related to the angular velocity ω. From $\omega=2\pi n/60$, the angular velocity ω could be converted into the rotational speed n of blade roller. Referring to GB/T5668-2017 "Rototiller", rotational speed n was taken in the range of 150-350 r/min. In summary, the angular velocity ω will affect the stability of adhering soil. To determine the effect of angular velocity ω on adhering soil, the rotary speed n was selected as the simulation test factor based on the conversion relationship between angular velocity ω and rotational speed n.

3.3 Analysis of the contact time between rotary blade and soil during rotary tillage

The occurrence of soil adhesion process between blade roller and soil in the rice stubble field extended outward over time from around the contact point. It indicated that soil adhering blade roller was also a function of time[21]. Therefore, based on the analysis of contact time between rotary blade and soil, the equation of rotary blade cutting trajectory under different tillage depths was constructed. The parameters influencing soil adhering to staggered blade rollers were determined. As shown in Figure 5, rotary blades with different tillage depths were considered as research subjects (h_1>h_2). The coordinate system XOY was established at the center point O of blade shaft, and the forward direction of machine and vertical ground direction were X and Y axis respectively. Rotary blade 1 cut soil with arc length of L_{A1A2} and tillage depth h_1. Similarly, rotary blade 2 cut soil with arc length of L_{A3A4} and tillage depth h_2. The time t_1, t_2 for rotary blade 1 passing through points A_1, A_2 and the time t_3, t_4 for rotary blade 2 passing through points A_3, A_4 were calculated as follows.

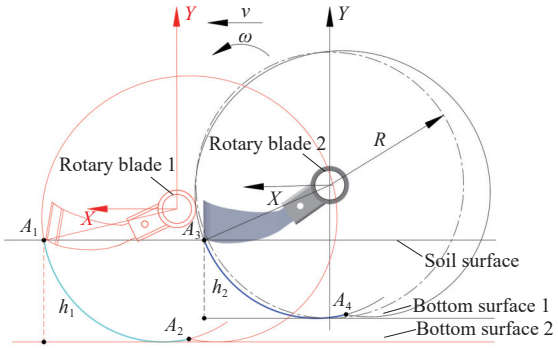

Figure 5 Analysis of soil contact processes of rotary blades with different tillage depths

$$\begin{cases} t_1 = \dfrac{\arcsin\left(1 - \dfrac{h_1}{R}\right)}{\omega} \\ R\cos(\omega t_2) + v t_2 = \dfrac{3\pi v}{2\omega} \\ t_3 = \dfrac{\arcsin\left(1 - \dfrac{h_2}{R}\right)}{\omega} \\ t_4 = t_2 \end{cases} \tag{12}$$

where, v is forward velocity of machine, m/s; t is cutting time, s.

The times t_2 and t_4 could be obtained from Equation (12) and the cutting pitch s.

$$R\cos(\omega t) + \frac{s\omega t Z_2}{2\pi} = \frac{3sZ_2}{4} \tag{13}$$

It was assumed that the contact moment between the rotary blade and topsoil surface in a single rotation cycle was a, and the completion moment of cutting the soil slice was b. The arc length L from time a to time b, and the interaction time T between rotary blade and soil from entering to separating are shown in Equation (14).

$$\begin{cases} L = \displaystyle\int_a^b \sqrt{v^2 - 2vR\omega\sin(\omega t) + R^2\omega^2}\,dt \\ T = \dfrac{\pi - 2\arcsin\left(1 - \dfrac{h}{R}\right)}{\omega} \end{cases} \tag{14}$$

Combined with the above analysis, it could be concluded that t_2–t_1>t_4–t_3, L_{A1A2}>L_{A3A4}. Consequently, we could also found that the greater the tillage depth h made longer the cutting time t. The cutting arc length L and interaction time T will increase. When rotary tillage operation, it was necessary to reduce the tillage depth h to prevent the soil from adhering to the blade roller. Nevertheless, a variety of cropping systems such as rice-wheat, rice-oil and rice-rice coexisted in the middle and lower reaches of the Yangtze River agricultural region. Crop cultivation agronomy needed to meet the requirements of different tillage depths h. The cutting pitch s affected the cutting time t and changed the probability of adhesion between blade roller and soil. The angular velocity ω of rotary blade became larger, so that the interaction time T became shorter. If the angular velocity ω was so faster, the soil disturbance will be greater, and the soil thrown by the front blade roller will easily collide with the rear blade roller and adhering to it. Moreover, the angular velocity ω could convert the rotational speed n. In summary, the rotational speed n, cutting pitch s and tillage depth h were selected as the simulation test factors for soil adhesion.

3.4 Design of staggered rotary blade arrangement

Staggered rotary blades arrangement was required to avoid motion interference, for which the sidelong section edge of rotary blades spatial coordinate system was established. As shown in Figure 6, a fixed coordinate system *oxyz* was established at the intersection of lengthwise section plane and rear blade shaft. The fixed coordinate system *oxyz* were moved along the *x*-axis direction with a distance of rotary radius *R*. Then, it was rotated 30° (sliding angle of rotary blade[22]) around the positive direction of *x*-axis. The coordinate system $o_0x_0y_0z_0$ for the sidelong section edge of rotary blade Ⅰ on rear blade roller was obtained. The fixed coordinate system *oxyz* were moved along the *x*-axis direction with a distance of l_1-*R*cos(π–λ), moved along the *y*-axis direction with a distance of *R*sin(π–λ), moved along the *z*-axis direction with a distance of D_1. Eventually, it was rotated 210° around the positive direction of *x*-axis, and the coordinate system $o_1x_1y_1z_1$ was established for the sidelong section edge of rotary blade Ⅲ on front blade roller. According to the rotation and translation transformations of the coordinate systems $o_0x_0y_0z_0$, $o_1x_1y_1z_1$ and *oxyz*, the Equations (15) and (16) were shown below:

$$\begin{bmatrix} x \\ y \\ z \end{bmatrix} = \begin{bmatrix} 1 & 0 & 0 \\ 0 & \sin 30^\circ & \cos 30^\circ \\ 0 & \cos 30^\circ & -\sin 30^\circ \end{bmatrix} \begin{bmatrix} x_0 \\ y_0 \\ z_0 \end{bmatrix} + \begin{bmatrix} vt + R\cos\omega t \\ -R\sin\omega t \\ 0 \end{bmatrix} \tag{15}$$

$$\begin{bmatrix} x \\ y \\ z \end{bmatrix} = \begin{bmatrix} 1 & 0 & 0 \\ 0 & \sin(\pi+30^\circ) & \cos(\pi+30^\circ) \\ 0 & \cos(\pi+30^\circ) & -\sin(\pi+30^\circ) \end{bmatrix} \begin{bmatrix} x_1 \\ -y_1 \\ z_1 \end{bmatrix} + \begin{bmatrix} vt + R\cos(\omega t-\lambda) + l_1 \\ -R\sin(\omega t-\lambda) \\ D_1 \end{bmatrix} \tag{16}$$

where, λ is lag angle of two rotary blades with different bending directions of adjacent sections, (°); D_1 is distance between the two blade holder cross sections in the case of single blade roller, mm.

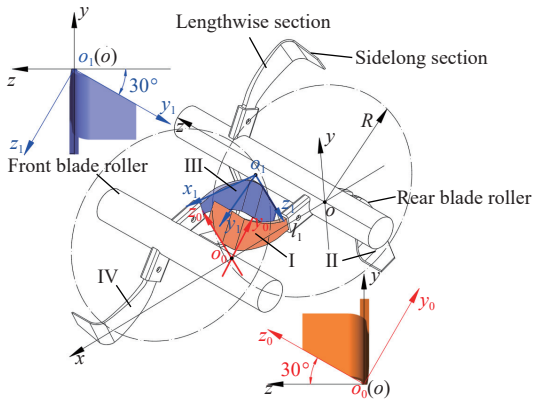

a. Spatial coordinate for the sidelong section edge of rotary blade

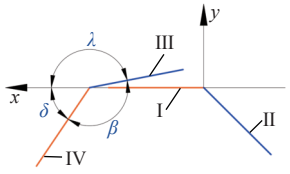

b. The angle relationship of staggered rotary bladein *xoy* plane

Figure 6 Spatial coordinate construction for the sidelong section edge of staggered rotary blade

The width of common rotary blade was about 50mm, and the distance between the two blade holder cross section was greater than rotary blade width. Two rotary blades were installed on the same cross section with different bending directions. For this reason, the distance D_1 between the two blade holder cross section in the case of a single blade roller was determined to be 120 mm. Rotary blades installed on the single blade roller were distributed to the front and rear blade rollers to form a staggered arrangement. The distance D_2 between the two adjacent blade holder became twice the previous distance. The total number of rotary blades installed and the angle of axially adjacent rotary blades in the same direction were calculated as follows[23]:

$$\begin{cases} Z_1 = \dfrac{1000BZ_2}{b} \\ \beta = 4 \times \dfrac{360^\circ}{Z_1} \end{cases} \tag{17}$$

where, Z_1 is total number of rotary blades, and the resulting value is an even number; Z_2 is number of rotary blades on the same blade holder cross section; *B* is blade roller width, m; *b* is distance between two cross section of adjacent blade holder, mm; β is angle of axially adjacent rotary blades in the same direction, (°).

Bring the values into Equation (17) to find the total number of rotary blades Z_1 was 26. The angle of axially adjacent rotary blade in the same direction β was 55.38°. For processing convenience, the value of β was taken as 56°, which satisfied the requirement of β in the range of 54°≤β<85°. In the axial direction, the angle δ between two rotary blades installed in the same cross section should be greater than 90°, where the angle δ was chosen to be 135°. Within a single rotary cycle, rotary blade Ⅰ and Ⅲ overlap once. When the *z*-axis coordinates of two points on the sidelong section edge of rotary blades Ⅰ and Ⅲ were equal, the trajectories of the two points in the *xoy* plane were as follows:

$$\begin{cases} x_0 = vt + R\cos(\omega t) \\ y_0 = -R\sin(\omega t) \\ x_1 = vt + R\cos(\omega t - \lambda) + l_1 \\ y_1 = -R\sin(\omega t - \lambda) \end{cases} \tag{18}$$

According to GB/T5668-2017 “Rototiller” obtained rototiller forward speed, rotational speed of 0.3-1.4 m/s and 150-350 r/min respectively. The forward speed and rotational speed were selected as (0.3, 150), (0.85, 250) and (1.4, 350) respectively. It was taken as the theoretical calculation values into Equation (18), and the time function about *t* was solved simultaneously. The equations of trajectories for staggered rotary blades in a single rotation cycle is shown in Figure 7. The results showed that there was no real number solution of the equation, it demonstrated that there was no interference during the motion of staggered rotary blades. The rotary blades were arranged reasonably. Through the above analysis, the arrangement of staggered rotary blades is shown in Figure 8.

4 Materials and methods

4.1 Test design and measurement of simulation

The EDEM software was used to construct the simulation model of rotary tillage based on discrete element method. The prediction model between key factors and soil adhesion mass was established by response surface design method. In the middle and lower reaches of the Yangtze River, the rotational speed and soil cutting pitch were determined under different requirements of planting agronomic tillage depth, reducing the soil adhesion mass. In the meantime, the process of soil particles adhering staggered blade rollers and rotary blades scraping off the adhering soil were

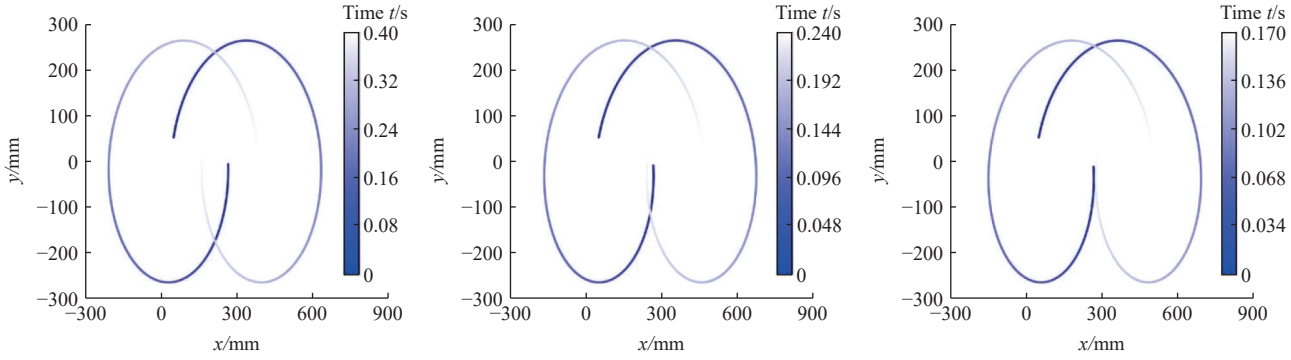

a. v=0.30, n=150 b. v=0.85, n=250 c. v=1.40, n=350

Figure 7 The spatial and temporal trajectory changes for the sidelong section edge of staggered rotary blades

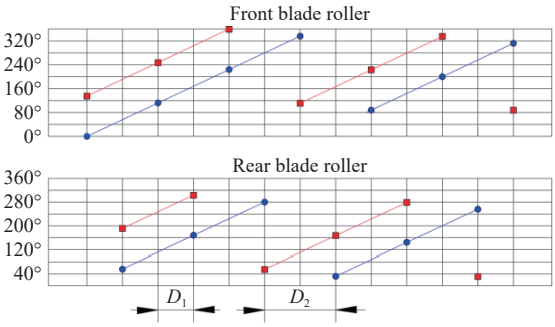

Figure 8 Arrangement of rotary blades on the front and rear blade rollers

clarified

Based on the analysis in section 3, Box-Behnken simulation test was conducted. The rotational speed n, cutting pitch s and tillage depth h were taken as the test factors and the soil adhesion mass was selected as the response value. As listed in Table 1, the rotational speed simulation range was 150-350 r/min. To ensure the quality of tillage, soil moisture content was controlled by sunning and irrigation after rice harvest, and the rotary tillage cutting pitch s was taken in the range of 6-10 cm[24]. The tillage depth of different crops in the middle and lower reaches of the Yangtze River ranged in 10-20 cm, which was taken as the simulation range of tillage depth. The machine forward velocity v was solved according to the cutting pitch s and rotational speed n (v=ns/3000).

Table 1 Experimental factors codes

Code	rotational speed n/(r·min^{-1})	Cutting pitch s/cm	tillage depth h/cm
−1	150	6	10
0	250	8	15
1	350	10	20

The simulation contact model and its parameters were determined by integrating the findings of the previous study, leading to the establishment of the machine-soil discrete element simulation model[25]. The simulation was conducted on the left half of the machine, considering its symmetrical center side, with the soil box dimensions set at 3000 mm×1500 mm×300 mm. Upon completion of the simulation, the quantity of soil adhering to the front and rear blades and shafts was measured. The EDEM post-processing module was utilized to obtain the number of particles adhering to different parts. Finally, the soil adhesion mass Q was calculated based on the mass of individual particles and the total number of particles. The simulation model is shown in Figure 9.

4.2 Experimental conditions and methods of field experiments

The field experiment was conducted on October 2021 at the experimental field of the Institute of Grain Crops, Hubei Academy of Agricultural Sciences (114°18′E, 30°29′N). The experimental field, with clay loam soil, was planted with rice all year round. Among experimental field, the soil moisture content of experimental field Ⅰ was higher than the field Ⅱ and Ⅲ, with moisture content ranging from 29.79% to 35.88%. The straw height in field Ⅰ and Ⅱ was 30-40 cm, which laid down on the ground. The straw height in field Ⅲ was 30-45 cm, which erected on the surface. The physical parameters before tillage for the three fields is listed in Table 2.

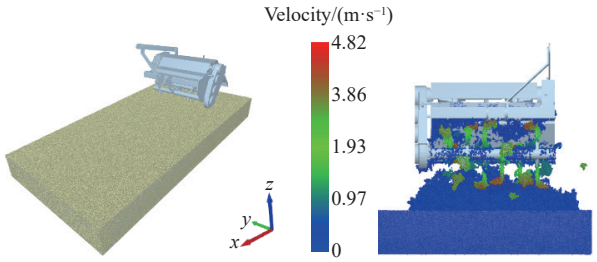

a. Simulation model b. Soil particle adhering blade rollers

Figure 9 Discrete element simulation model of rotary tillage

Table 2 Physical properties of the experimental field before tillage

Experimental field number	Physical Properties			
	Soil moisture content/%	Amount of straw cover/(g·m^{-2})	Straw moisture content/%	Weight capacity/(g·cm^{-3})
Ⅰ	33.78	904	23.46	1.58
Ⅱ	22.90	780	22.57	1.52
Ⅲ	23.13	820	18.23	1.55

The experimental instruments were as follows: the ARSDS, DFF1204 and LX908 tractor, comprehensive performance test vehicle for field operation equipment, electronic balance, etc. The experimental field is shown in Figure 10.

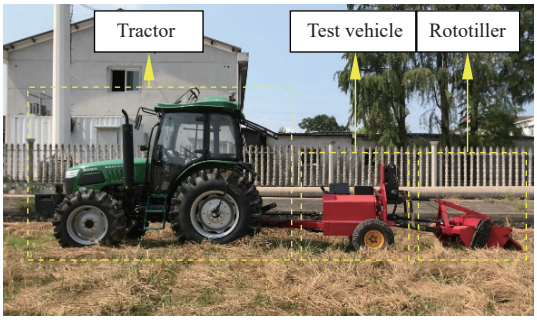

Figure 10 Field experiment

The soil in the middle and lower reaches of the Yangtze River was wet and slippery, and the tractor was prone to slippage. During operation, the tractor forward velocity 1 (V1) and velocity 2 (V2) were set to (1.62±0.20) km/h and (2.76±0.20) km/h, respectively, and rotational speed was stable at 230r/min. The working distance was 40 m per travel in a straight line. The stable measurement area, 20 m in the middle, was selected to test the working quality of the machine. Each group of experiments was repeated for 3 travels.

At the end of each experimental travel, the machine was lifted by three-point suspension device. The mixture of soil and straw adhering to the staggered blade rollers was scraped and its mass was weighed using an electronic balance as the soil adhesion mass. The average value of soil adhesion mass for 3 travels under each group of experiments was counted.

Referring to GB/T5668-2017 "Rototiller" standard, the operating power consumption, post-tillage levelness, tillage depth, tillage depth stability as well as straw burial rate performance indexes were measured for each experimental travel.

5 Results and discussion

5.1 Results and analysis of simulation

5.1.1 Results of simulation

The maximum, middle and minimum values of the test factors were selected for the three levels of high, medium and low in the Box-Behnken response surface test design, respectively. A total of 17 sets of simulations were performed in the EDEM software, with 5 repetitions of the central horizontal group (Table 3). Eventually, the experimental results were processed to obtain the prediction model of rotational speed n (X_1), cutting pitch s (X_2) and tillage depth h (X_3) and soil adhesion mass Q.

Table 3 Experiment scheme and results

Test No.	Test factors			Soil adhesion mass Q/g
	X_1	X_2	X_3	
1	150	6	15	5512
2	350	6	15	5448
3	150	10	15	5001
4	350	10	15	4891
5	150	8	10	4134
6	350	8	10	4197
7	150	8	20	7293
8	350	8	20	6781
9	250	6	10	4261
10	250	10	10	3856
11	250	6	20	7170
12	250	10	20	6738
13	250	8	15	5027
14	250	8	15	5037
15	250	8	15	4965
16	250	8	15	5065
17	250	8	15	5055

The experimental results were analyzed by quadratic regression and fitted by multiple regression to check the significance of each factor effect on the response value. As listed in Table 4, the prediction model reached a significant level (p<0.01), and the lack of fit was not significant (p>0.05). The model correction coefficient was 0.9972, suggesting that the model had good reliability. Analysis of the experimental factors showed that X_1, X_2, X_3, X_1X_3, X_1^2 and X_3^2 had a highly significant effect on soil adhesion mass. The prediction model of each significant factor with the soil adhesion mass Q was calculated as follows:

$$Q = 5029.8 - 77.87X_1 - 238.13X_2 + 1441.75X_3 - 143.75X_1X_3 + 139.1X_1^2 + 432.35X_3^2 \quad (19)$$

Table 4 Significant analysis of the prediction model for soil adhesion mass

Source of variation	Sum of square	Degrees of freedom	Mean square	F	p
Model	1.81×10^7	9	2.02×10^6	625.72	<0.0001**
X_1	4.85×10^4	1	4.85×10^4	15.06	0.0060**
X_2	4.54×10^5	1	4.54×10^5	140.85	<0.0001**
X_3	1.67×10^7	1	1.66×10^7	5163.40	<0.0001**
X_1X_2	5.29×10^2	1	5.29×10^2	0.16	0.6974
X_1X_3	8.27×10^4	1	8.27×10^4	25.67	0.0015**
X_2X_3	1.82×10^2	1	1.82×10^2	0.057	0.8188
X_1^2	8.15×10^4	1	8.15×10^4	25.30	0.0015**
X_2^2	8.19×10^3	1	8.19×10^3	2.54	0.1548
X_3^2	7.87×10^5	1	7.87×10^5	244.38	<0.0001**
Residual	2.25×10^4	7	3.22×10^3		
Lack of fit	1.64×10^4	3	5.47×10^3	3.57	0.1255
Pure error	6.13×10^3	4	1.53×10^3		
Total	1.82×10^7	16			

Note: ** indicates a highly significant effect.

5.1.2 Analysis of model interaction effects and optimization

From the experimental results, it could be concluded that the blade roller rotational speed and tillage depth had an interaction effect on soil adhesion mass. As can be seen from Figure 11, the cutting pitch was located at the center level, the soil adhesion mass was basically the same with the increase of rotational speed when the tillage depth was 10-15 cm. When the tillage depth was greater than 15 cm, the soil adhesion mass decreased with the increase of rotational speed, and the rate of decrease was obvious. When the rotational speed was certain, the soil adhesion mass showed a significant increased with the increase of tillage depth. The tillage depth was less than 15 cm resulting in less soil adhesion mass. Soil particles were directly adhering to the surface of blade rollers, and the centrifugal force was not obvious. Higher rotational speed led to large soil disturbance by the blade roller, and the dropped soil tended to adhere to the blade shaft, causing an increase in soil adhesion mass. After the tillage depth was greater than 15cm, the soil adhesion mass became larger because of the contact area between blade rollers and soil increased. The greater the rotational speed caused the stronger the centrifugal force to make the soil break away from the blade roller.

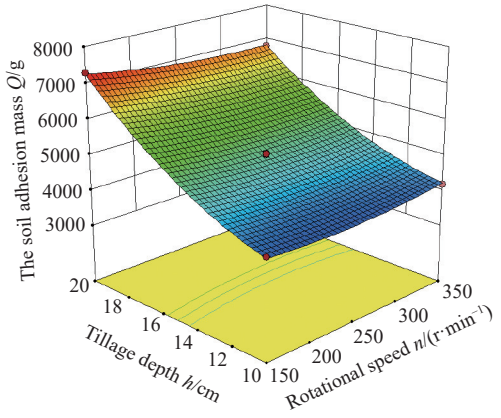

Figure 11 Effect of interaction on the soil adhesion mass on staggered blade rollers

With the optimization objective of reducing the soil adhesion mass, the multi-objective variable optimization algorithm was used to solve Equation (19) that obtained the optimal combination of parameters. The minimum soil adhesion mass was 3983.21 g when the rotational speed was 263.46 r/min, the cutting pitch was 8.43 cm, and the tillage depth was 10.00 cm. In order to verify the accuracy of optimization results, the rotational speed of 260 r/min, the cutting pitch of 8.50 cm and the tillage depth of 10.00 cm were selected in consideration of the actual operation. The soil adhesion mass was 3988.83 g in re-simulation results, representing basically consistent with the theoretical results. According to the prediction model developed, the optimal working parameters for different crop tillage depths could be predicted. For subsequent field validation of the prediction model accuracy, the tillage depth of wheat cultivation in the middle and lower reaches of the Yangtze River was taken as 14 cm[26]. The optimal combination of parameters was determined as 229.27 r/min of rotational speed and 10cm of cutting pitch, in which case the soil adhesion mass was 4584.62 g. when taken the rotational speed 230 r/min and re-simulation, the soil adhesion mass was 4566.67 g, it had a relative error of 0.39%. The above results were generally consistent with the predicted results of the prediction model.

5.1.3 Analysis of the process of staggered rotary blades scraping off adhering soil

The staggered double-roller consisted of a front blade (rotary blade and blade holder on the front blade roller), a front shaft, a rear blade (rotary blade and blade holder on the rear blade roller), and a rear shaft. From Figure 12, it could be obtained that the soil adhesion mass: rear blade > front blade > rear shaft > front shaft. The soil adhesion mass of rear blade, front blade and rear shaft increased rapidly in the initial moments of the simulation until it tended to stabilize. The soil adhesion mass of front blade and front shaft was lower than that of the rear shaft and rear blade, respectively. The soil was thrown backward by the front blade roller, and the soil contacted the rear blade roller to accelerate the soil adhering to the surface of rear blade and shaft, so that the soil adhesion mass of rear shaft was larger than the front shaft. The front and rear blades cut the soil periodically, and the process of adhesion-detachment-adhesion occurred with the soil. As a result, the soil adhesion mass of front and rear blades increased sharply and then stabilized.

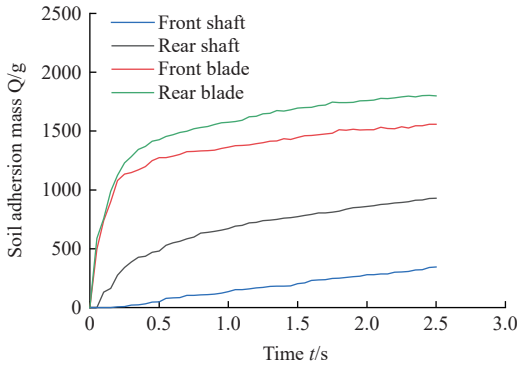

Figure 12 Changes of the soil adhesion mass with time in different parts of staggered blade rollers

During one cycle, soil started to adhere to the blade rollers. Then, the adhering soil was scraped off by the rotary blades, ensuring that soil did not accumulate on the blade roller. In the whole range of simulation parameters and under different parameter combinations, the cutting circles formed by the front and rear blades will scrape the adhering soil. Therefore, the staggered blade rollers could achieve the effect of soil detachment during the tillage operation. The blade scrapes off the soil that adhere to the blade rollers in single cycle as shown in Figure 13.

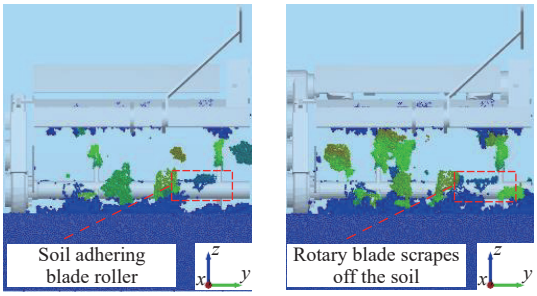

a. 1.8 s b. 2.2 s

Figure 13 The blade scrapes off the soil that adhere to the blade rollers in single cycle

5.2 Results and analysis of field experiments

5.2.1 analysis of soil adhesion mass

The soil adhesion mass produced by the staggered blade rollers was mainly straw mass in field Ⅱ and Ⅲ, which was concentrated in the sidelong section of rotary blade. There was basically no straw wrapping around the blade shaft (Figure 14). Compared with field Ⅲ, more soil was mixed with straw wrapping around the sidelong section of rotary blade in field Ⅱ. The soil and straw formed a complex with the rotary blade that created an interfacial adhesion. It is easier to accumulate on the rotary blade. After operation in field Ⅰ, the soil adhesion masses were 16.710 kg and 13.455 kg for two forward velocities (Table 5).

As shown in Figure 15, in the field Ⅰ, the ARSDS concentrated the soil adhesion mass on the sidelong section of rotary blades. The straw and soil complex was wrapped around the sidelong section and was not easily detached. There was no adhering and clogging soil in blade rollers. After the operation of conventional rototiller, the soil gradually adhered and accumulated on the blade roller until it was consistent with the rotary radius, which led the operation effect significantly worse. The average value of soil adhesion mass for conventional rototiller was measured as 38.215 kg.

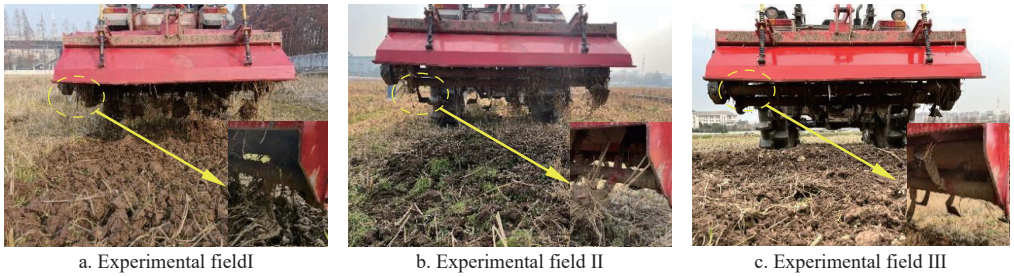

a. Experimental fieldI b. Experimental field II c. Experimental field III

Figure 14 The soil adhesion mass in different experimental fields of the ARSDS

Table 5 Soil adhesion mass measurement results

Experimental field number	I		II		III	
Forward velocity	V1	V2	V1	V2	V1	V2
Average value of soil adhesion mass/g	16 710	13 455	1855	895	330	230

Note: V1= (1.62±0.20) km/h, V2= (2.76±0.20) km/h.

a. ARSDS b. Conventional rototiller

Figure 15 Comparison of soil adhesion mass between ARSDS and conventional rototiller

5.2.2 Analysis of tillage depth and tillage depth stability

The tillage depths of 18.28 cm and 18.05 cm were significantly higher in the high moisture content field Ⅰ than other fields. The coefficients of tillage depth stability were 87.95% and 86.73% for field Ⅰ, 89.12% and 90.45% for field 2, and 89.32% and 88.07% for field 3, respectively. The tillage depth stability was relatively worse in the field 1. The measurement results are shown in Figure 16.

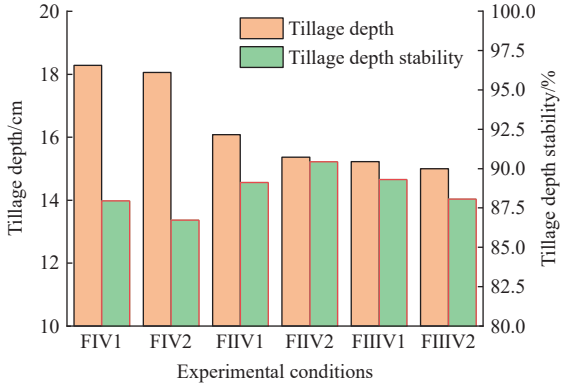

Figure 16 Results of tillage depth and tillage depth stability

5.2.3 Analysis of post-tillage levelness, power consumption and straw burial rate

The soil in the field Ⅰ were not easily separated from each other. The soil thrown by the blade rollers was mostly agglomerated. Soil volume was larger than in the low moisture content field. During the measurement, it was found that the soil blocks in field Ⅰ were irregular shape. Large gaps between the soil blocks resulted in large fluctuations in the measured post-tillage levelness values within each tillage travel.

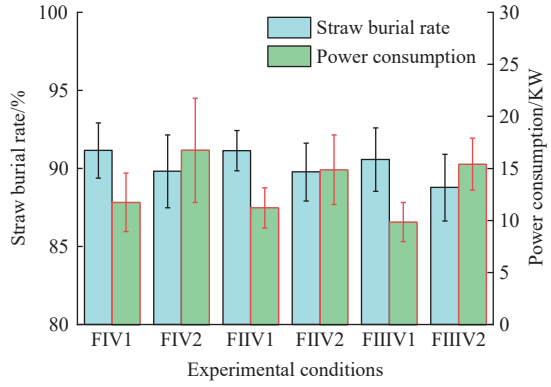

Figure 17 Results of power consumption and straw buried rate measurements

The measurement results of power consumption and straw burial rate are shown in Figure 17. The power consumption of field Ⅰ was greater than both the field Ⅱ and Ⅲ. Straw burial rate of more than 90% was achieved in all three field at low velocity. The experimental results are listed in Table 6. It can be seen that that the maximum post-tillage levelness was 2.46 cm, the maximum power consumption was 16.75 kW, and the straw burial rate was greater than 88%. The experiments found that the ARSDS had low power consumption. It was because of the low soil capacity, and the fact that the number of rotary blades on the staggered double-roller was the same as on the single-roller. The experimental indexes all meet GB/T5668-2017 "Rototiller" standard.

Table 6 Results of post-tillage levelness measurements

Experimental field number	I		II		III	
Forward velocity	V1	V2	V1	V2	V1	V2
Post-tillage levelness/cm	2.42	2.46	1.32	1.75	1.50	2.42

6 Discussion

This study confirms that the anti-adhesion rototiller, employing staggered double-roller scraping, effectively reduces soil adhesion, as evidenced by theoretical design, simulation tests, and field experiments. The soil adhering to the blade rollers is scraped off by the staggered blades on the front and rear blade shafts during movement, disrupting the equilibrium and facilitating soil detachment through blade extrusion and centrifugal force. Importantly, this staggered arrangement does not require additional scraping devices or blades, maintaining the same blade count as a single-roller rototiller. With blades set at a certain angle, the front and rear rotary blades do not interfere with each other during rotation. Simulation test results demonstrate that rotary blades successfully detach adherent soil from the blade rollers in one cycle, preventing soil accumulation. Additionally, the machine meets operational requirements in field experiments.

It was observed that soil adhesion mass in the high moisture content field was notably greater compared to the low water content field. This is attributed to the water film tension at the interface between the soil and the blade rollers, affecting soil adhesion. As the soil absorbed water and reached its plastic limit, the adhesion between interfaces strengthened with increasing moisture content. Related studies have indicated a significant increase in the magnitude of adhesion force after the moisture content surpassed 30%[27]. Prior to each experiment, the tractor's three-point suspension was adjusted to achieve a predetermined tillage depth. However, it was discovered that the actual average tillage depths exceeded the predetermined tillage depth. Interaction between the tractor and the soil led to soil subsidence and alterations in soil physical properties[28]. The sinking of tractor tires caused the machine to lower in height. Nevertheless, the height of the soil surface unaffected by tire contact remained constant, resulting in a tillage depth exceeding the predetermined value. Consequently, the actual height of the blade shaft from the surface decreased, leading to direct contact between the soil and the blade rollers, resulting in adhesion. Furthermore, the trajectory of the rotary blade resembled a residual pendulum, exerting an uplifting effect on the cultivated soil during rotary tillage. Soil with high moisture content and strong plasticity tends to maintain its shape upon contact with the blade roller. Simultaneously, soil was ejected in the forward direction. The ejected soil tended to aggregate, elevating the surface height and promoting adhesion to the blade rollers.

The experiments verified that the method of staggered scraping with rotary blades achieved significant anti-adhesion and detachment effects, even under different moisture content and operating conditions, effectively addressing the issue of soil adhesion accumulation. Consequently, the research findings can provide a theoretical basis and technical support for the design of anti-adhesion in rototiller.

7 Conclusions

In response to the problem of soil adhesion of blade roller in rice stubble field, the ARSDS was designed by mechanical scraping methods. Rotary blade scraping off the soil that adhered to the blade roller was achieved. The main conclusions were drawn as below.

The key parameters that affect the soil adhering on and separating from the blade roller were determined to be the rotational speed, cutting pitch and tillage depth. Rotary blades installed on the single blade roller were distributed to the front and rear blade rollers to form a staggered arrangement.

Using discrete elements to simulate the soil adhering blade rollers process, the optimal combination of parameters for a tillage depth of 14 cm was determined to be 230 r/min for rotational speed and 10 cm for cutting pitch. The simulation results showed that the soil adhesion mass increased rapidly at the beginning until it stabilized. The staggered blade rollers were able to effectively scrape off the adhering soil in the whole range of simulation parameters and with different combinations of parameters.

The anti-adhesion rototiller based on staggered double-roller scraping could effectively solve the problem of soil adhering blade roller when compared to conventional rototiller in rice stubble field with high moisture content. The field experiments were carried out to verify the operation performance of ARSDS. The results showed that the stability of tillage depth was greater than 86%, the maximum flatness after tillage was 2.46 cm, the maximum power consumption was 16.75 kW, and the straw burial rate was greater than 88%.

Acknowledgements

This work was supported by the National Natural Science Foundation of China (Grant No. 32271994, 31901412), Hubei Provincial Natural Science Foundation (Grant No. 2024AFB696). The authors thank the editors and the anonymous reviewers for their constructive suggestions on the paper.

[References]

[1] Xu G M, Wang X C, He R Y, Ding Q S. Performance evaluation of rotary tillage straw returning based on composite indicators and measurement techniques. Transactions of the CSAM, 2022; 53(2): 58–67. (in Chinese)

[2] Huang W, Hall S J. Elevated moisture stimulates carbon loss from mineral soils by releasing protected organic matter. Nature Communications, 2017; 8(1): 1–10.

[3] Nguyen B T, Lehmann J. Black carbon decomposition under varying water regimes. Organic Geochemistry, 2009; 40(8): 846–853.

[4] Wang J, Xiong Z, Kuzyakov Y. Biochar stability in soil: meta‐analysis of decomposition and priming effects. Global Change Biology Bioenergy, 2016; 8(3): 512–523.

[5] Cheshomi A, Jafari M, Rajabi A M. Results of cone and piston pull-out tests for evaluation of clay-soil adhesion. Soil and Tillage Research, 2023; 225: 105552.

[6] Zhang D G, Zuo G B, Tong J, Zhang Z H, Experiment and optimization of sub-soil liquid fertilizer injection device. Transactions of the CSAE, 2020; 36(1): 31–39. (in Chinese)

[7] Ren L Q, Wang Y P, Li J Q, Tong J. The flexible unsmoothed cuticles of soil animals and their characteristics of reducing adhesion and resistance. Chinese Science Bulletin, 1998; 43(2): 166–169.

[8] Luo W, Wang J K, Luo X Y, Niu H L, Duan W X, Li Y, et al.Improved design and experiment of profiling and recycling plastic film mechanism for clamping finger-chain type device of recycling residual plastic film. Transactions of the CSAE, 2017; 33(22): 27–35. (in Chinese)

[9] Liu G, Xia J, Zheng K, Cheng J, Wang K, Zeng R, Wang H, Liu, Z. Effects of vibration parameters on the interfacial adhesion system between soil and metal surface. Soil and Tillage Research, 2022; 218: 105294.

[10] Ma Y H, Ma S S, Jia H L, Liu Y C, Peng J, Gao Z H. Measurement and analysis on reducing adhesion and resistance of bionic ripple opener. Transactions of the CSAE, 2014; 30(5): 36–41. (in Chinese)

[11] Guan C, Fu J, Xu L, Jiang X, Wang S, Cui Z. Study on the reduction of soil adhesion and tillage force of bionic cutter teeth in secondary soil crushing. Biosystems Engineering, 2022; 213: 133–147.

[12] El Salem A, Zhang G, Wang H, Salem H M, Abdalla M A, Ghazy A A. The effect of integrating a bio-inspired convex structure with a low-surface energy polymer on soil adhesion and friction. Journal of Terramechanics, 2023; 109: 93–100.

[13] Marani S M, Shahgholi G, Moinfar A. Effect of nano coating materials on reduction of soil adhesion and external friction. Soil and Tillage Research, 2019; 193: 42–49.

[14] Matin M A, Hossain M I, Gathala M K, Timsina J, Krupnik T J. Optimal design and setting of rotary strip-tiller blades to intensify dry season cropping in Asian wet clay soil conditions. Soil and Tillage Research, 2021; 207: 104854

[15] Xiao M H, Wang K X, Yang W, Wang W C, Jiang F. Design and experiment of bionic rotary blade based on claw toe of Gryllotalpa orientalis Burmeister. Transactions of the CSAM, 2021; 52(2): 55–63. (in Chinese)

[16] Sun J, Chen H, Wang Z, Ou Z, Yang Z, Duan J. Study on plowing performance of EDEM low-resistance animal bionic device based on red soil. Soil and Tillage Research, 2020; 196: 104336.

[17] Li Y W, Zhang G Y, Zhang Z, Zhang Y, Hu T D, Cao Q Q. Development of low power-consumption multi-helical rotavator for small vertical-shaft deep-cultivator. Transactions of the CSAE, 2019; 35(4): 72–80. (in Chinese)

[18] Hu J P, Zhao J, Pan H R, Liu W, Zhao X S. Prediction model of double axis rotary power consumption based on discrete element method. Transactions of the CSAM, 2020; 51(S1): 9–16. (in Chinese)

[19] Yoshida S, Adachi K, Hosokawa H. Analysis of seasonal change in paddy soil structure based on the elasto-plastic deformation model. Geoderma, 2014; 228: 104–113.

[20] Xu B Y. Concise elasticity and plasticity. Beijing: Higher Education Press, 2011. (in Chinese)

[21] Xu L, Lio A, Hu J, Ogletree D F, Salmeron M. Wetting and capillary phenomena of water on mica. The Journal of Physical Chemistry B, 1998; 102(3): 540–548.

[22] Zhang C L, Chen L Q, Xia J F, Zhang J M. Effects of blade sliding cutting angle and stem level on cutting energy of rice stems. Int J Agric & Biol Eng, 2019; 12(6): 75–81.

[23] Feng P Z. Optimum number-sequence arrangement of rotary-tiller blades. Journal of Jiangsu Institute of Technology, 1985; 4: 40–49. (in Chinese)

[24] China Academy of Agricultural Mechanization Sciences. Agricultural machinery design manual: Volume I. Beijing: China Agricultural Science and Technology Press, 2007; (in Chinese)

[25] Cheng J, Zheng K, Xia J F, Liu G Y, Jiang L, Li D. Analysis of adhesion between wet clay soil and rotary tillage part in paddy field based on discrete element method. Processes, 2021; 9(5): 845.

[26] Cheng S H, Guo W S, Wang L J. Wheat in South China. Nanjing: Jiangsu Science and Technology Press, 2012. (in Chinese)

[27] Ren L Q. Soil adhesion mechanics. Beijing: China Machine Press, 2011. (in Chinese)

[28] Benoit O, Gotteland P. Modelling of sinkage tests in tilled soils for mobility study. Soil and Tillage Research, 2005; 80(1-2): 215–231.